International Journal of Sciences

Research Article Volume 13 – June 2024 (06)

Numerical Investigation of Flow Characteristics on Camera Side Mirrors in Vehicles

Emre Ulutaş[1], Onur Yemenici[1]

[1]Department of Mechanical Engineering, University of Uludag, Turkey

Abstract: In this study, the flow characteristics affecting camera side mirrors, which are used in modern concept vehicles and electric vehicles, were numerically investigated. Additionally, a slot was designed parallel to the flow surface in the camera side mirror model, and the effect of the slot on the drag coefficient was examined. The analyses were conducted at speeds of 20 m/s, 30 m/s, and 40 m/s, using the SST k-ω turbulence model. The computational domain was 800 mm in width, 800 mm in height, and 1200 mm in length, with the mirror positioned 400 mm from the inlet. The analyses showed that the drag coefficient decreased as the speed increased for all mirror models. The maximum improvement in the drag coefficient was observed at a speed of 40 m/s with Model1 camera side mirror with a slot. The drag coefficient values for Model1 camera side mirrors with and without a slot were 45.8% and 33.4% lower, respectively, compared to the traditional mirror.

Keywords: Camera Side Mirror, Computational Fluid Dynamics (CFD), Drag Coefficient, Aerodynamics

1. Introduction

Side mirrors used in vehicles are among the most critical safety features, allowing drivers to see the surroundings of the vehicle and thereby minimizing the risk of accidents. The drag coefficient in automobiles is determined based on the shape and aerodynamic properties of the vehicle. The aerodynamic design of side mirrors affects the vehicle's drag coefficient. Properly designed and appropriately positioned side mirrors play a significant role in reducing the vehicle's air resistance, thereby enhancing fuel efficiency. In light of this information, non-optimized side mirrors can disrupt the aerodynamic profile of the vehicle, leading to an increase in the drag coefficient. Therefore, optimization studies in side mirror designs are crucial. This is especially important for electric vehicles and high-performance cars, where aerodynamic performance is paramount, making the design and improvement of side mirrors highly significant.

Camera side mirrors are a modern technology that can replace traditional side mirrors by providing a wider field of view, thereby improving the visibility of blind spots, reducing aerodynamic drag to increase fuel efficiency, and enhancing driver safety in adverse weather conditions. Consequently, camera side mirrors have been the subject of various studies in recent years. For example, in a study by Yu et al. [1], different mirror models with various surface curves were analyzed on 25 types of curves and 9 types of surfaces to create Class A surfaces on side mirrors and investigate their impact on drag coefficient. Keleşoğlu [2] conducted aerodynamic analyses on a simplified heavy commercial vehicle model with four different mirror models at speeds of 10, 15, 20, and 25 m/s. By identifying the regions of aerodynamic resistance on the camera side mirror (Model 1) and applying passive flow control methods, aerodynamic improvements were achieved. The study concluded that the aerodynamic drag coefficient decreased by 4.24% for Model 2 compared to the traditional mirrored model and by 0.96% compared to Model1. For Model3, the drag coefficient decreased by 6.24% compared to the traditional mirrored model and by 1.13% compared to Model1. In another study, İpci [3] examined the effects of conventional side mirrors and side view cameras on the aerodynamic drag coefficient of an urban bus model. At free flow speeds of 90 m/s and above, the drag coefficient was determined to be 0.539 for the bus with conventional side mirrors and 0.521 for the bus with side view cameras. The study found that the drag coefficient of a bus with conventional side mirrors was 6.6% higher than that of a mirrorless bus, and using cameras instead of mirrors reduced the drag coefficient by 3.45%. Arıkan [4] scanned a vehicle's side mirror with a 3D scanner to obtain its geometry and analyzed the aerodynamic drag coefficient at speeds of 80, 100, and 120 km/h. He created three different side mirror models for comparison and investigated the optimal mirror model form. The study concluded that the trapezoidal model was the most aerodynamically efficient, while the rectangular model was the least efficient. Ensarioğlu [5] investigated the aerodynamic forces and flow structures affecting four different side mirror designs at speeds of 20 m/s, 30 m/s, and 40 m/s, and at yaw angles of -10°, 0°, and 10°.

This article is published under the terms of the Creative Commons Attribution License 4.0
Author(s) retain the copyright of this article. Publication rights with Alkhaer Publications.
Published at: http://www.ijsciences.com/pub/issue/2024-06/
DOI: 10.18483/ijSci.2769; Online ISSN: 2305-3925; Print ISSN: 2410-4477

Emre Ulutaş, Onur Yemenici (Correspondence)
+

Additionally, he examined the effect of the mounting arm geometry for two of the models. In their study, Sadat et al. [6] examined the drag coefficients of traditional mirrors and camera side mirrors. They found that camera side mirrors, due to their smaller frontal area, improved the overall aerodynamics of the vehicle, reducing drag force by 2.6%. Zulhazmi et al. [7] conducted analyses of two different side mirrors, a reference model side mirror, and an internally ducted side mirror, at speeds of 100 km/h, 130 km/h, and 150 km/h. They concluded that the internally ducted side mirror was a better design for reducing aerodynamic resistance.

In this study, the flow structure and drag coefficients of traditional side mirrors, camera side mirrors, and camera side mirrors with internal slots were numerically investigated at flow speeds of U=20 m/s, 30 m/s, and 40 m/s.

2. Methodology

In this research, the design of traditional side mirrors, camera side mirrors, and camera side mirrors with slots was carried out using the CATIA software, while the computational fluid dynamics analyses were conducted using the ANSYS FLUENT software.

To achieve the objectives of the research and confirm its accuracy, verification was performed using literature studies. The mirror model used in the numerical study by Yu et al. [1] was modeled with the same dimensions for verification purposes. Figure 1 shows the reference model and computational domain used in the verification study. The computational domain dimensions are 800 mm in width, 800 mm in height, and 1200 mm in length, with the mirror positioned 400 mm from the inlet.

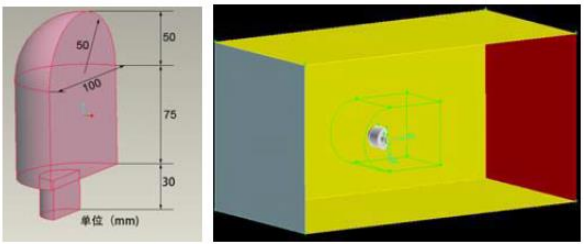

Figure 1. Reference model and computational domain used in the verification study [1]

As the inlet boundary condition, a speed of 30 m/s was used, and zero pressure gradient was set as the outlet boundary condition. The SST k-ω turbulence model was selected for the analyses. The SST k-ω turbulence model is a two-equation model used to simulate complex turbulent flow fields, boundary layers, and separation phenomena. This model combines the standard k-ω model with the shear stress transport (SST) model. The SST k-ω turbulence model is defined by the following equations for turbulence kinetic energy (k), turbulence frequency (ω), and turbulence viscosity (μ_t). The equations for turbulence kinetic energy, turbulence frequency, and turbulence viscosity are given in Equations [1], [2], and [3], respectively.

Equation for turbulence kinetic energy (k):

$$\frac{\partial(\rho k)}{\partial t}+\frac{\partial(\rho u_i k)}{\partial x_i}=P_k-\beta^*\rho k\omega+\frac{\partial}{\partial x_i}\left[(\mu+\sigma_k\mu_t)\frac{\partial k}{\partial x_i}\right] \quad (1)$$

Equation for turbulence frequency (ω):

$$\frac{\partial(\rho\omega)}{\partial t}+\frac{\partial(\rho u_i\omega)}{\partial x_i}=\alpha\frac{\omega}{k}P_k-\beta\rho\omega^2+\frac{\partial}{\partial x_i}\left[(\mu+\sigma_\omega\mu_t)\frac{\partial\omega}{\partial x_i}\right]+2(1-F_1)\rho\sigma_{\omega2}\frac{1}{\omega}\frac{\partial k}{\partial x_i}\frac{\partial\omega}{\partial x_i} \quad (2)$$

Equation for turbulence viscosity (μ_t):

$$\mu_t=\frac{\rho k}{\omega}\max\left(1,\frac{0.31\eta}{SF_2}\right) \quad (3)$$

The mirror surface and the walls of the created analysis domain were treated as smooth surfaces, and the Coupled algorithm was employed as the solution method. To enhance the accuracy and reliability of the results, a dense mesh was applied around the mirror, and a local volume was created within the computational domain. The polymesh grid structure was selected as the mesh model. In the study by Yu et al. [1], the drag coefficient of the side mirror was determined to be C_D=0,452, while in the validation study, it was found to be C_D=0,455.

Figure 2 depicts the mesh structure of Model1 camera side mirror within the flow volume. As a result of the mesh independence studies, for the analysis of Model1 camera side mirror, the number of nodes was determined to be 4084818, the number of surfaces 5117975, and the number of mesh cells 734804. Figure 3 presents the graph of the mesh independence study.

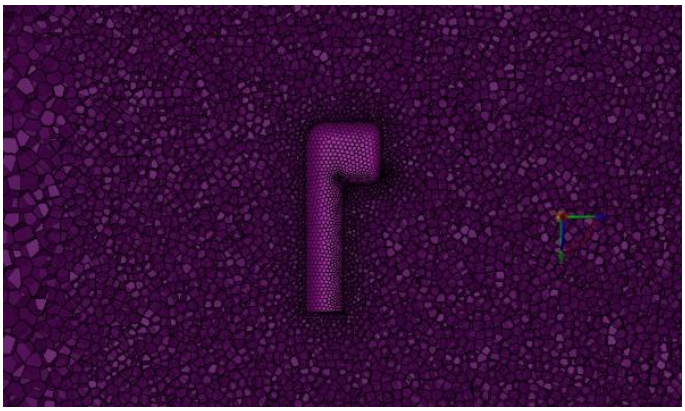

Figure 2. Mesh structure of model1 with camera side mirror

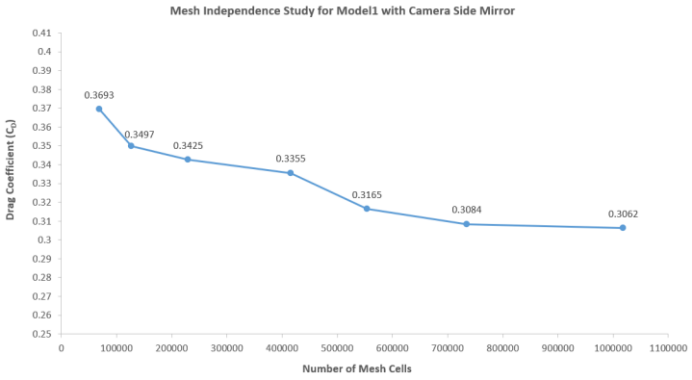

Figure 3. Mesh independence study for model1 with camera side mirror

In Figure 4, the flow volume and mesh structure of Model1 with slotted camera side mirror are detailed. For the analysis of Model1 with slotted camera side mirror, the node count is determined as 4230338, surface count as 5297377, and mesh cell count as 761198.

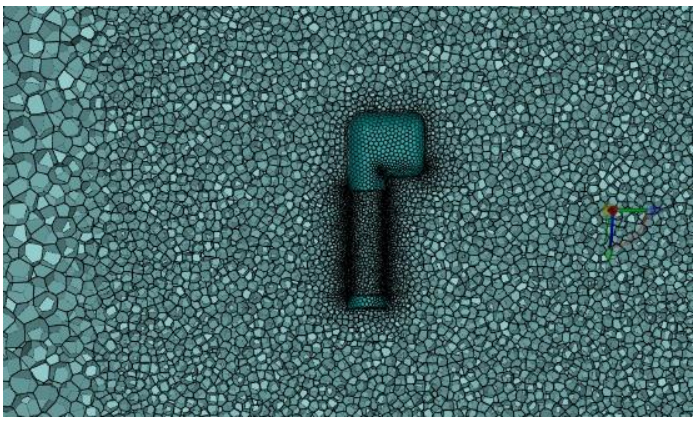

Figure 4. Mesh structure of model1 with slotted camera side mirror

The geometric models and dimensions of Model1 and Model1 with slotted camera side mirrors to be used in the analyses are given in Figure 5 and Figure 6, respectively.

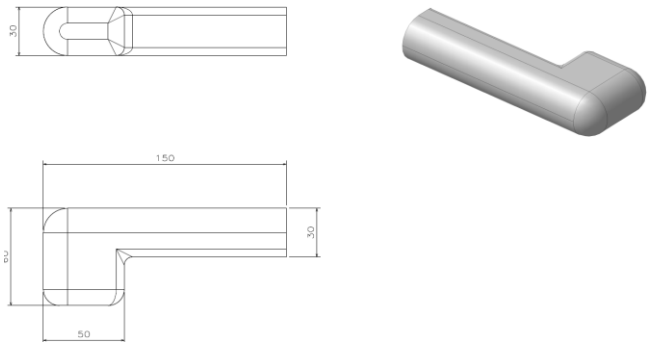

Figure 5. Model1 camera side mirror model

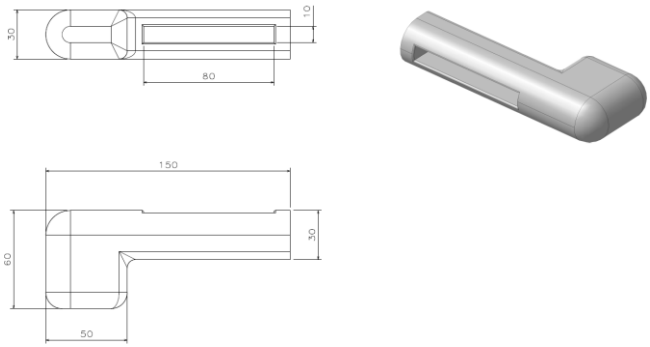

Figure 6. Model1 slotted camera side mirror model

The drag coefficients were obtained by conducting analyses of the camera side mirror model and its slotted version at flow velocities of 20 m/s, 30 m/s, and 40 m/s. The SST k-ω turbulence model was used in the analyses. Details of the parameters used in the analyses are shown in Table 1.

Table 1. Analysis conditions and convergence criteria

Parameter	**Description**
Velocity inlet, v	20 m/s, 30 m/s, 40 m/s
Pressure outlet	0 kPa
General	
Type	**Pressure-Based**
Velocity Formulation	Absolute
Time	Steady
Mesh	Poly
Model	
Viscous	SST k-ω
Material	
Fluid	
Density of air	1.225 kg/m^3
Methods	
Scheme	Coupled
Gradient	Least Squares Cell Based
Pressure	Second Order
Momentum	Second Order Upwind
Turbulent Kinetic Energy	Second Order Upwind
Specific Dissipation Rate	Second Order Upwind

Convergence Criterion	
Continuity	10^{-4}
Velocity (x-y-z)	10^{-6}
k	10^{-5}
ω	10^{-5}
Initialization	
Methods	Standart
Turbulent Kinetic Energy	1.851482 m^2 / s^2
Specific Dissipation Rate	12675 1/s

3. RESULTS AND DISCUSSION

In this section, flow structures and drag coefficients on a camera side mirror model were investigated at flow velocities of 20 m/s, 30 m/s, and 40 m/s. Additionally, the effect of adding slots parallel to the flow surface on the drag coefficient of the camera side mirror model was observed. Results from traditional mirrors were compared with those from camera side mirrors in the validation study.

Figures 7, 8, and 9 depict the magnitude of velocities in the flow over the traditional mirror, Model1 camera side mirror, and Model1 slotted camera side mirror, respectively, at a velocity of 30 m/s.

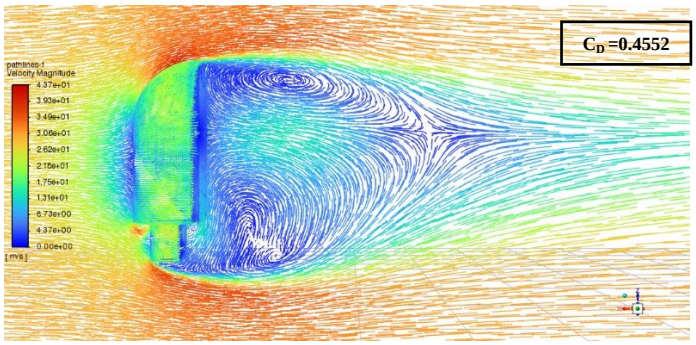

Figure 7. Magnitude of flow velocities over traditional mirror at 30 m/s velocity

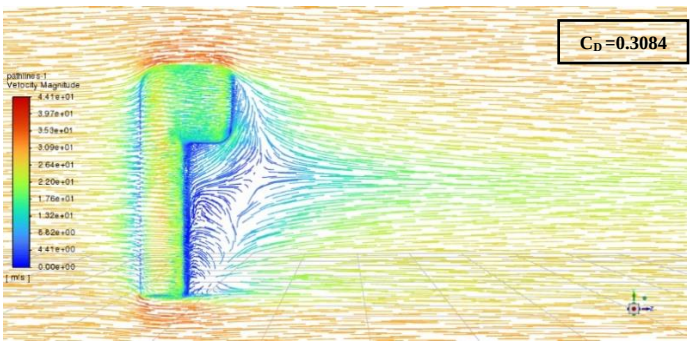

Figure 8. Magnitude of flow velocities over model1 camera side mirror at 30 m/s velocity

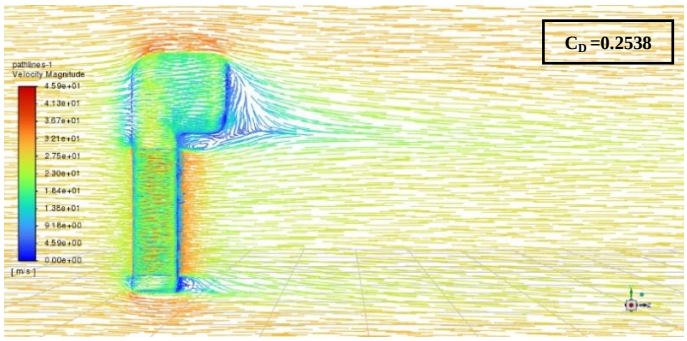

Figure 9. Magnitude of flow velocities over model 1 slotted camera side mirror at 30 m/s velocity

According to the analysis results for Model1, Model1 slotted, and traditional side mirrors, it was observed that the velocity is zero around the midpoint of the mirror where the flow first impacts, while it is maximum at the edges of the mirror. Particularly in the case of the traditional mirror, a significant decrease in velocity and intense vortex formations were observed in the region behind the mirror. Compared to the traditional mirror, the Model1 camera side mirror exhibited a reduction in vortex intensity in the region behind the mirror. With the Model1 slotted side mirror, the opening of slots substantially mitigated the formation of vortices behind the mirror.

The variation of the drag coefficient C_D in the flow over Model1, Model1 slotted, and traditional side mirrors at flow velocities of 20 m/s, 30 m/s, and 40 m/s is presented in Figure 10.

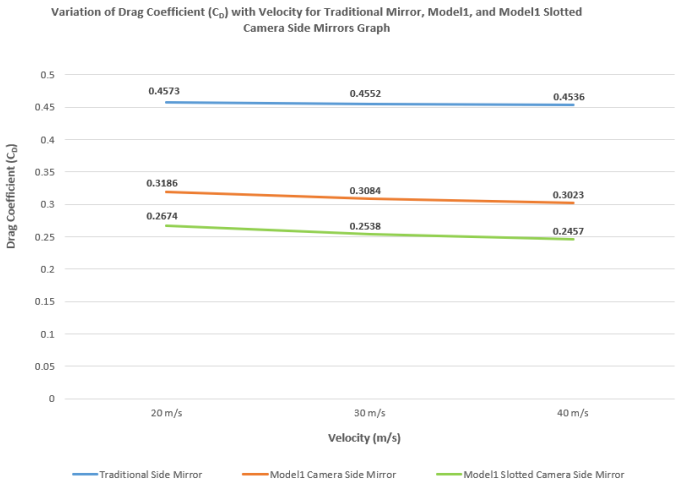

Figure 10. Variation of drag coefficient (C_D) in traditional mirror, Model1, and Model1 slotted side mirrors

When examining the C_D coefficient values at 20 m/s velocity, it's observed that Model1 and Model1 slotted camera side mirrors provide improvements of approximately 30.3% and 41.5%, respectively, compared to the traditional mirror. The Model1

slotted camera side mirror value shows an improvement of 16.1% over Model1, owing to the slots opened on the side mirror. At flow velocities of 30 m/s and 40 m/s, the drag coefficient values in the Model1 camera side mirror are respectively 32.2% and 33.4% lower than those in the traditional mirror. The drag coefficient values of the Model1 slotted camera side mirror are 44.2% and 45.8% lower than those of the traditional mirror for flow velocities of 30 m/s and 40 m/s, respectively. The minimum C_D coefficient values in the flow were obtained at 40 m/s velocity for Model1, Model1 slotted, and traditional side mirrors.

4. Conclusion

This study investigates the flow over a camera-equipped side mirror model at flow velocities of 20 m/s, 30 m/s, and 40 m/s. Additionally, the effect of creating a slot on the camera-equipped side mirror to examine its impact on the flow was studied, and all results were compared with those of a traditional side mirror. The summarized results are as follows:

• As the velocity increased, the drag coefficient C_D values decreased in all side mirror models.

• In the traditional mirror, the intensity of vortices behind the mirror was significantly higher compared to Model1 camera-equipped side mirrors, where this intensity notably decreased in the area behind the mirror.

• Flow over the Model1 slotted side mirror showed that the presence of the slot prevented the formation of vortices behind the mirror.

• The C_D values for velocities of 20 m/s, 30 m/s, and 40 m/s were as follows: in the traditional mirror: 0.4573, 0.4552, and 0.4536; in Model 1 side mirror: 0.3186, 0.3084, and 0.3023; and in Model 1 slotted side mirror: 0.2674, 0.2538, and 0.2457, respectively.

• Considering design criteria, the best result was achieved with the Model1 slotted side mirror.

References

1. G. Yu and D. Liu, “Numerical analysis on the relationship between aerodynamic drag coefficient and 3d molding of rear view mirror,” *CCIE 2011 - Proc. 2011 IEEE 2nd Int. Conf. Comput. Control Ind. Eng.*, vol. 1, pp. 117–121, 2011, doi: 10.1109/CCIENG.2011.6007971.
2. O. KELEŞOĞLU, “Ağır Ticari Bir Araçta Farklı Yan Ayna Modellerinin Aerodinamik Yapıya Etkilerinin Nümerik Olarak İncelenmesi,” vol. 4, no. 1, pp. 88–100, 2023.
3. D. İPCİ, “A Comparative CFD Study of Side-view Mirror and Side-view Camera Usages on a City Bus,” *Int. J. Automot. Sci. Technol.*, vol. 4, no. 3, pp. 138–143, 2020, doi: 10.30939/ijastech..726376.
4. M. ARIKAN, “Otomobillerdeki Yan Aynaların Dış Yüzeyinde Oluşan Hava Direnci Etkisinin Nümerik Olarak İncelenmesi,” *SELL J.*, vol. 5, no. 1, p. 55, 2020.
5. M. V. ENSARİOĞLU, “Taşıtlarda Yan Ayna Üzerindeki Aerodinamik Etkilerin Nümerik Olarak İncelenmesi,” vol. 4, no. 1, pp. 9–15, 2017.
6. M. Sadat, N. Albab, F. Chowdhury, and M. M. A. Khan, “Numerical Simulation Approach to Investigate the Effects of External Modifications in Reducing Aerodynamic Drag on Passenger Vehicles,” *Int. J. Automot. Mech. Eng.*, vol. 19, no. 1, pp. 9563–9576, 2022, doi: 10.15282/ijame.19.1.2022.19.0738.
7. A. N. Zulhazmi and N. Mustaffa, “The Effect of Inner Duct on Aerodynamic Noise of an Outside Rear View Mirror,” *J. Automot. Powertrain Transp. Technol.*, vol. 1, no. 1, pp. 1–5, 2021, doi: 10.30880/japtt.2021.01.01.006.